JOURNAL OF MATERIALS SCIENCE 31 (1996) 5069–5075

TEM study of kaolinite thermal decomposition by controlled-rate thermal analysis

F. BERGAYA, P. DION, J.-F. ALCOVER
Centre de Recherche sur la Matière Divisée, CNRS-Université d'Orléans, 1b rue de la Férollerie 45071 Orléans Cedex 2, France

C. CLINARD, D. TCHOUBAR
Centre de Recherche sur la Matière Divisée, CNEA, Université d'Orléans BP 6759-45067 Orléans Cedex 2, France

The dehydroxylation of kaolinite leading to metakaolinite was studied by transmission electron microscopy. TEM techniques allow the study of morphology, structure (by selected-area electron diffraction) and lattice imaging (by high resolution) in a non-destructive way. The samples were prepared using a controlled-rate thermal analysis method which provides a well-defined material (near thermodynamic equilibrium). The dehydroxylation begins near the defects of the structure (stacking defects, dislocation and edges) and progresses from them slowly, producing metakaolinite without any intermediate state. The formed metakaolinite is still organized: the two-dimensional hexagonal structure of the *ab* plane remains, but with a shorter extension ($\approx$50 nm). A lamellar structure of a few layers with an interlayer period of about 1.2 nm appears in place of the kaolinite layers (0.71 nm). This structure is explained by the tetrahedral SiO_4 sheet which remains but is highly deformed by a distortion wave due to the new aluminium and oxygen (remaining from the OH sheet) distribution after the loss of water.

1. Introduction

Thermal transformation of kaolinite leading to metakaolinite is a very important step prior to the formation of mullite in ceramic or porcelain processing. The mechanisms of dehydroxylation in the kaolinite samples have been studied [1, 2] using controlled-rate thermal analysis (CRTA), and the local structure of the samples has been analysed [1, 3] by solid-state high-resolution nuclear magnetic resonance (MASNMR). The transmission electron microscopy using selected-area electron diffraction (SAED) and lattice imaging (HRTM) is also very useful in that case. Until now, studies have been very scarce because this state of dehydroxylated kaolinite, called metakaolinite, is very brittle under the electron beam. However, with the technical progress in microscopy it is possible to reduce the rapid deterioration of the sample and to observe the actual structure. The great advantage of this technique is the ease with which domains of interest can be selected in the case of phase transformations which necessarily induce structural inhomogeneities in the samples partially transformed. In addition, it is possible to avoid impurity phase observation in natural samples.

2. Experimental procedure

2.1. Kaolinite structure

Kaolinite ($Al_4Si_4O_{10}(OH)_8$) [4] (Fig. 1a) is a 1:1 layer clay mineral which is built with a tetrahedral SiO_4 sheet and an octahedral $AlO_2(OH)_4$ sheet which are linked together by oxygen atoms. Moreover, the octahedral sheet contains some so-called internal OH groups inside the layer. The parameters of the tetrahedral sheet and those of the octahedral one have dimensions sufficiently close to adjust them together, and an octahedral–tetrahedral layer (1:1) extends in a two-dimensional array. The unit cell containing four tetrahedra and six octahedra is an ortho-hexagonal rectangle with $b \sim a3^{1/2}$. These layers are stacked and linked together essentially by hydrogen bonds between the external hydroxyls of the octahedral sheet, and the basal oxygens of the adjacent-layer tetrahedral sheet. The layer stacking is triclinic with $P\bar{1}$ space group. The parameters of the three-dimensional unit cell [5] are: $a = 0.515$ nm, $b = 0.894$ nm, $c = 0.740$ nm, $\alpha = 91.7°$, $\beta = 104.9°$, $\gamma = 89.8°$ and $d_{0\,0\,1} = 0.716$ nm. To ensure the electroneutrality of the structure, Al^{3+} cations are localized within the octahedral cavities, respectively named A, B, C (Fig. 1b). In the well-organized kaolinite, which is a dioctahedral silicate, only the A and C sites are occupied by the cations [4]. The B site corresponds to a vacancy. Fig. 1b shows, for an ideally hexagonal layer, the projection along the direction perpendicular to the layer plane, i.e. parallel to the reciprocal axis c^*.

2.2. Starting natural kaolinite and CRTA dehydroxylation process

The kaolinite "Gabriel" (UK) commonly used in the porcelain hostelry industry was used (this sample was

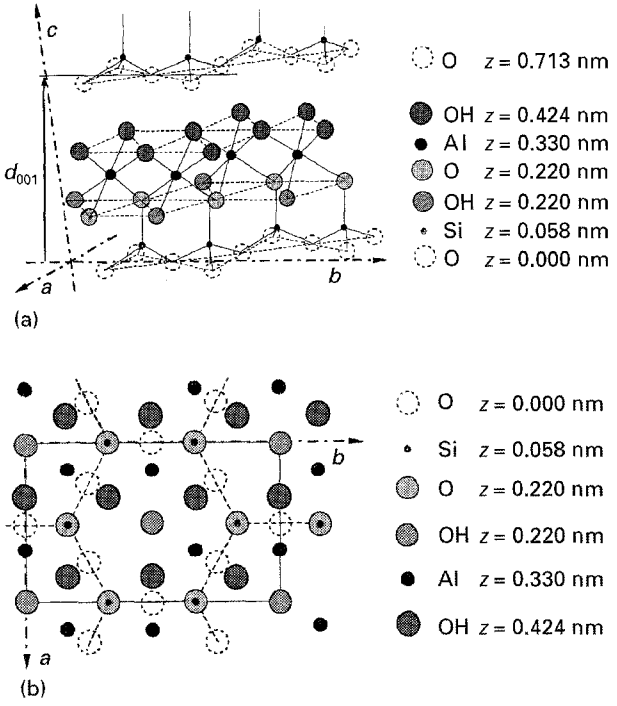

Figure 1 Structural model of kaolinite. (a) Visualization of the structure. (b) Orthogonal projection of the (*a*, *b*) plane showing the ideally hexagonal organization of SiO_4 tetrahedra and the position of the different sites A, B, C of the aluminium cations.

kindly provided by KPCL, Limoges, France). It contains 0.8 wt % Fe_2O_3 and between 10% and 15% impurities whose main constituent is a mica phase (muscovite).

Sample heating was carried out in a CRTA equipment (CTM-CNRS, Marseille, France) [6]. The sample was heated under constant gas flux extraction at constant pressure, which controls the increase of temperature. Using a very low gas (water) extraction rate (7.2×10^{-6} s^{-1} or 3.2 mg H_2O loss per hour for 1 g initial sample, at a constant pressure of 3×10^{-2} mbar) the sample was dehydrated in a quasi-thermodynamic equilibrium, self-regulated process that takes about 40 h for 1 g starting material. This is much slower than most of the classical thermal dehydroxylation techniques. At 850 °C the sample had lost its structural water. From the mass loss measurements it was possible to define precisely (better than 4%) the degree of dehydroxylation, α, of the sample (going from 0 to 1) as the fraction of H_2O loss at temperature T.

2.3. TEM Analysis: morphology, electron diffraction and lattice imaging

TEM observations of clay minerals generally lead to the same problems as met in the case of hydrates or oxyhydroxydes because they are easily disturbed by local heating induced by the impact of an electron beam under vacuum [7]. For example, kaolinite particles often present holes on transmission electron micrographs (Fig. 2a); in that case, the diffraction pattern disappears and is replaced by a diffused halo. It is now possible clearly to reduce this damage by decreasing the electron beam intensity or by increasing the

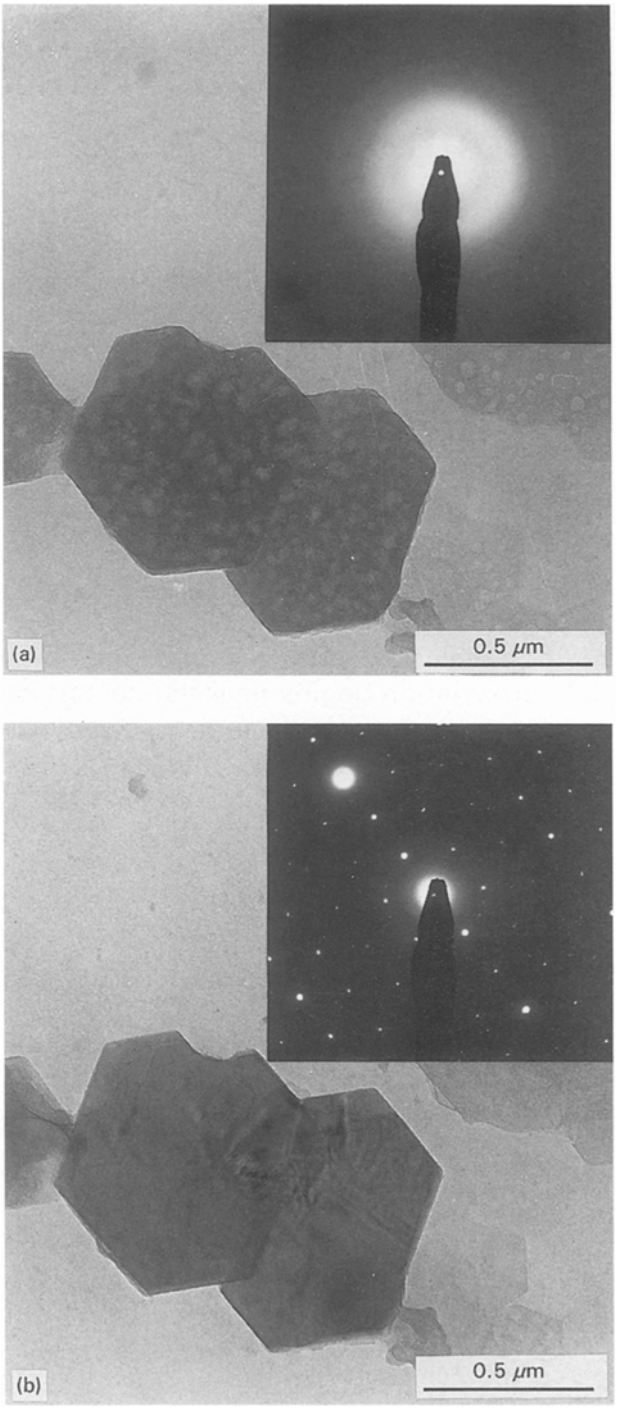

Figure 2 Bright-field image and electron diffraction diagrams of the starting sample kaolinite, (a) after damage by impact of the electron beam, and (b) normal.

electron acceleration voltage, in which case the structure is maintained, as in Fig. 2b.

Morphological observations, HRTM observations and SAED were performed in a TEM Philips CM20, equipped with a low-dose camera and which can work at 200 KV. Two types of observations were performed: (i) in the *ab* plane, samples were prepared by sedimentation. One drop of a very diluted clay dispersion (previously homogenized under ultrasounds) was deposited on a holey carbon film which was mounted on a 200 mesh 3 mm copper grid. After evaporation, the c^* axis is perpendicular to the support plane and thus parallel to the incident beam; (ii) in the c^* direction, an

inclusion technique [8], well adapted to these clay minerals, was used to obtain thin sections of about 50 nm in the direction perpendicular to the basal plane of the particles by using ultra microtomy.

3. Results

3.1. *ab* plane observations during the dehydroxylation process

3.1.1. Morphology

Bright-field observations of starting kaolinite particles show the classical hexagonal-shaped platelets (Fig. 2b). Such a morphology is not disturbed by the thermal treatment. The hexagonal outlines are only lightly rounded after heating at the highest temperatures (Fig. 3c,d).

3.1.2. Selected-area electron diffraction

In the starting kaolinite (Fig. 2b) the spots, distributed in a typical pseudo hexagonal symmetry of the kaolinite two-dimensional unit cell, are sharp and visible until the fourth order of reflection which is characteristic of a well-crystallized sample.

In kaolinite partially transformed (28%), as shown in Fig. 3a,b, the first step of dehydroxylation induces a decreasing number of visible reflections, which become broader. In addition, oriented diffuse scatterings (in the shape of butterflies) become visible relating, for example, the (1 1) reflection to the (0 2) one, or the (1 1) reflection to the (1 3) one.

When the degree of dehydroxylation is about 70% and when the transformation is complete (Fig. 3c,d), the diffuse scattering is progressively reduced to an isotropic halo. This halo is superimposed, with a light shift, on the six fundamental diffraction spots which remain in the diffractogram. This implies the conservation of the typical pseudo hexagonal symmetry of the kaolinite two-dimensional unit cell.

The evolution of the *b* parameter values during the dehydroxylation process was quantified from the (0 2) reflection positions with samples containing a gold

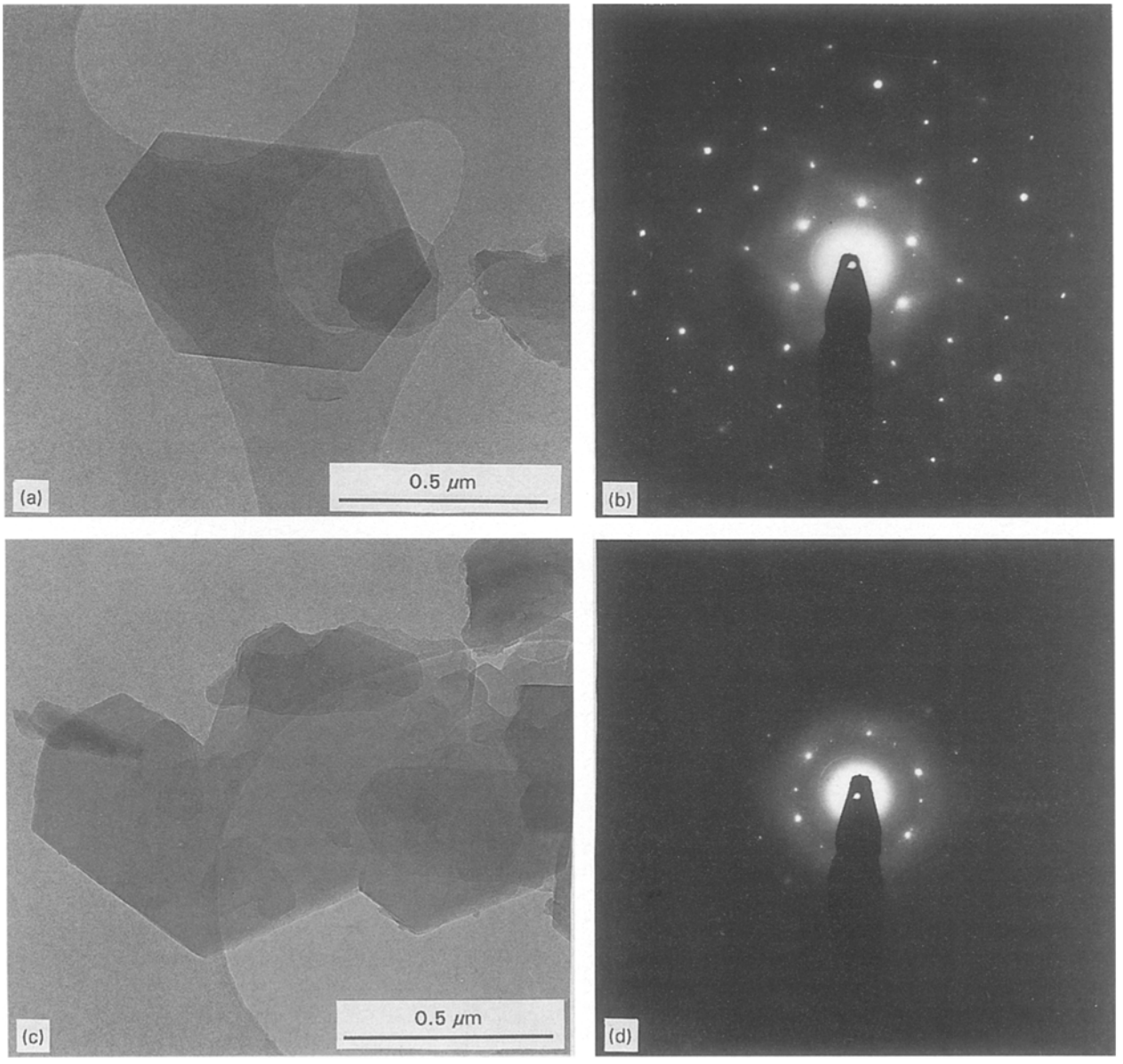

Figure 3 (a, c) Bright-field images and (b, d) electron diffraction diagrams of (a, b) kaolinite 28% transformed, and (c, d) "metakaolinite".

TABLE I

Temperature (°C)	Degree of transformation	*b* parameter (nm)
room	0	0.894
370	0.05	0.894
400	0.28	0.890
450	0.70	0.880
550	0.91	0.870
700	0.99	0.870
850	1	0.870

deposit as standard. The precision of the measurements was estimated at about 0.5%. The different *b* values as a function of temperature or the degree of transformation are given in Table I.

3.1.3. HRTM observations

In Fig. 4 the (0 2) fringes with an equidistance of 0.447 nm in non-transformed kaolinite and of 0.435 nm in the dehydroxylated phase (metakaolinite) are seen as revealed by HRTM. As shown in Fig. 4, the mean size of metakaolinite domains is about 50 nm.

3.2. Stacking of layers during the dehydroxylation process

The (0 0 1) lattice fringes were first observed for starting kaolinite and then during its thermal treatment at different transformation rates: 28% at 400 °C, 70% at 450 °C and 99% at 700 °C (Table I).

3.2.1. Starting sample

Fig. 5 shows two types of domains: (i) very well organized domains which are constituted by the fringes at 0.7 nm which are typical of well-crystallized kaolinite (Fig. 5a), and (ii) defect domains in which are concentrated thin and long lenses (arrows in Fig. 5b), whose thickness is about 0.9 nm and their lateral extension about 10 nm. Such defects were previously described by Plançon and Tchoubar [9]. Both kinds of domain can coexist within the same particle but the defect concentrations within the particles can be quite different.

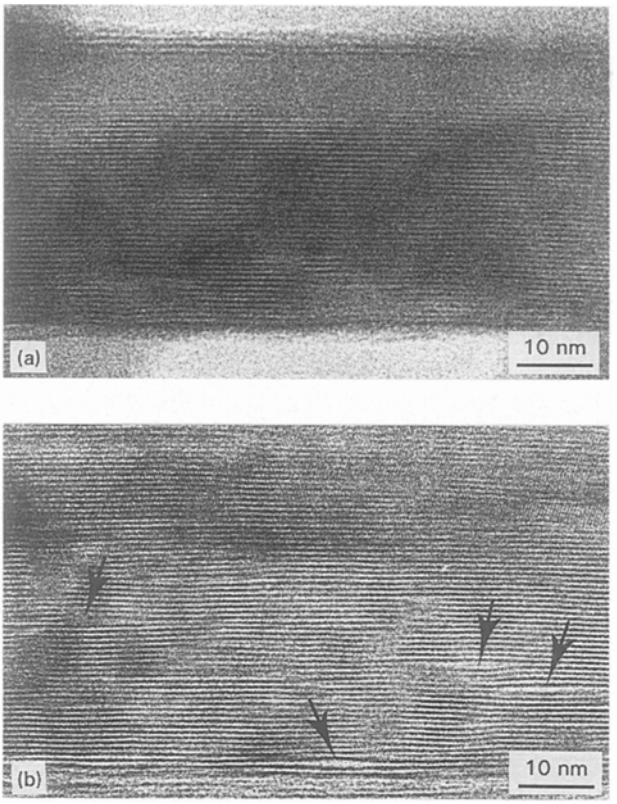

Figure 5 Lattice imaging (HRTM) of kaolinite (0 0 1) fringes: (a) kaolinite, very well organized; (b) kaolinite with defects.

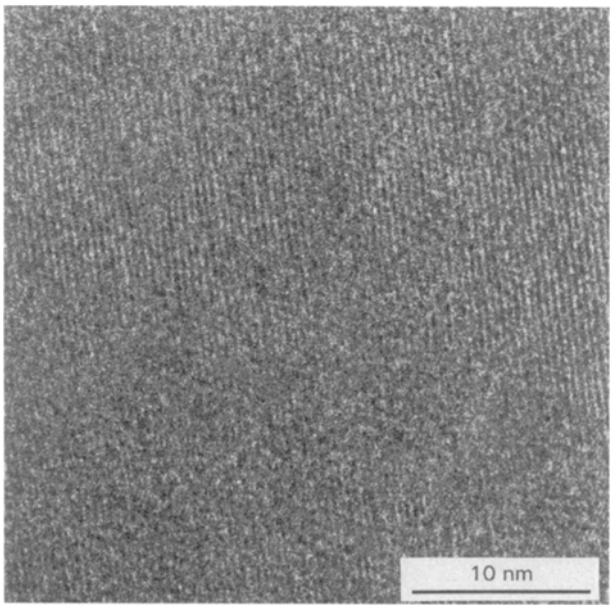

Figure 4 Lattice imaging (HRTM) of "metakaolinite" (0 2) fringes.

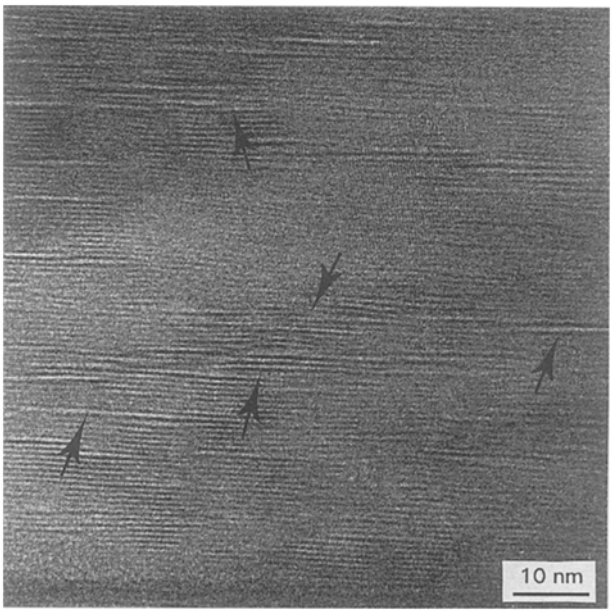

Figure 6 Lattice imaging (HRTM) of kaolinite 28% transformed, (0 0 1) fringes.

3.2.2. Sample 28% transformed

Fig. 6 shows the development of the lens lateral extension (until 30 nm) and also the breaking in plane of the kaolinite unit layer surrounding these defects (indicated by arrows). At this stage of transformation, the dehydroxylation mechanism starts almost from the defects.

3.2.3. Sample 70% transformed

This sample with a high transformation rate shows, once again, different domains. Fig. 7a shows domains highly transformed in which a new fringe family appears at 1.2–1.3 nm instead of the 0.7 nm fringes of the starting kaolinite. But also untransformed residual domains are still observed, corresponding to the best crystallized part of the starting sample (Fig. 7b). The dotted line indicates the frontier between transformed and untransformed domains.

3.2.4. Sample 99% transformed

This sample can be identified as pure metakaolinite. As expected, all the 0.7 nm fringes have disappeared and the 1.2–1.3 nm fringes are now only observable with a lateral extension at about 5 nm (Fig. 8).

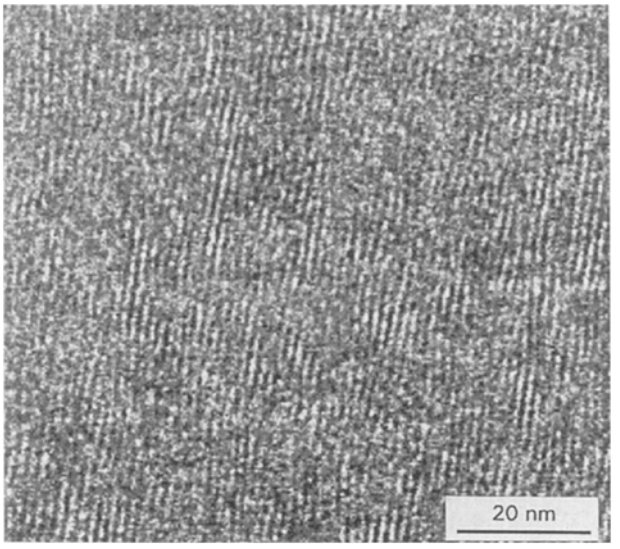

Figure 8 Lattice imaging (HRTM) of "metakaolinite" (0 0 1) fringes.

4. Discussion

4.1. Structural reorganization

The electron diffraction spots with hexagonal symmetry which are observed after dehydroxylation, show the persistence of a two-dimensional periodicity in the *a*, *b* plane of the metakaolinite layers. We have performed the same electron diffraction study on

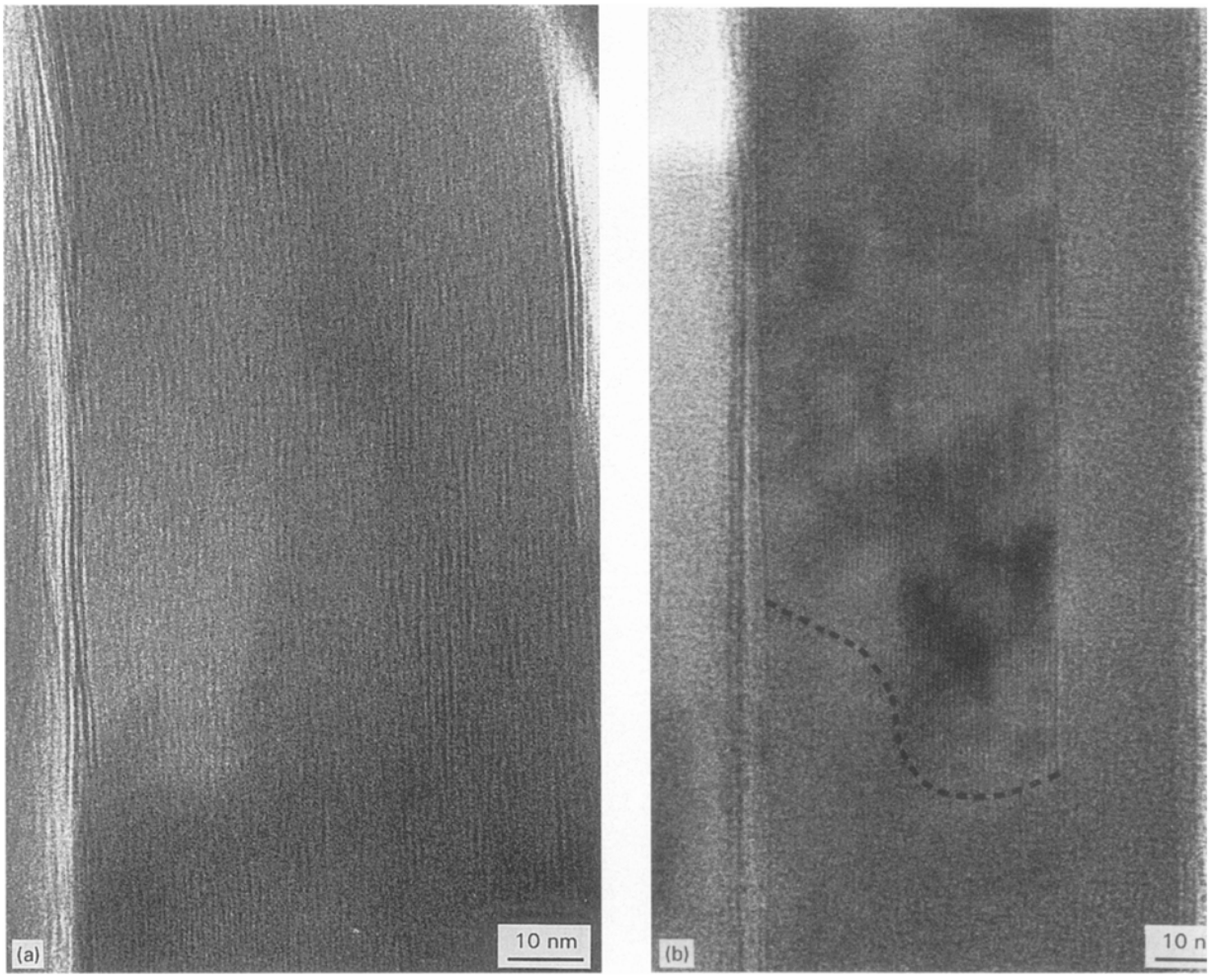

Figure 7 Lattice imaging (HRTM) of kaolinite 70% transformed, (0 0 1) fringes, showing (a) new fringes at 1.2–1.3 nm, and (b) untransformed domains.

samples which were obtained from a classical heating method, indicating a linear increase of temperature (1 °C min^{-1} until 850 °C), has lead to the same conclusions. This result is thus not dependent on the method of dehydroxylation and agrees with that obtained by Brindley *et al.* [10] from X-ray diffraction. It is worth recalling that such a result disagrees with those of Sonuparlak *et al.* [11], and Srikrishna *et al.* [12]. These authors report that the electron diffraction pattern of metakaolinite only shows a diffuse halo which is characteristic of an amorphous material. Such a difference in conclusions can be rightly explained by the great fragility of the dehydroxylated phase structure which can be easily broken down under the impact of the electron beam.

This two-dimensional long-distance ordering, which remains after dehydroxylation, is essentially stabilized by the SiO_4 tetrahedral sheet which does not contain the OH groups and, consequently, is not directly engaged in the dehydroxylation process. On the contrary, the structure of the octahedral sheet is submitted to an important bond recasting due to the OH lost.

Each OH has two aluminium cations and each aluminium cation has 4 OH and 2 O in their nearest environments (Fig. 1a and b) and therefore can lose $2H_2O$. It seems logical that the dehydroxylation begins between two adjacent OH which belong to the same octahedral edge.

For the first molecule of water removed, the dehydrolysis reaction can be written as

$$2(OH)\{\text{with } 2Al^{VI} \text{ in the nearest environment}\} \rightarrow H_2O(\uparrow) + O_{r1}\{\text{with } 2Al^{V}\} \quad (1)$$

where O_{r1} is the residual oxygen which remains bonded to the aluminium cation.

The aluminium cations which are concerned, have a five co-ordination, which was detected by NMR spectra of ^{27}Al in the same sample [3]. As discussed by Drits *et al.* [13] in the case of dehydroxylation of dioctahedral 2: 1 silicates where the residual oxygen is at the middle distance between the two previous sites, Al and O_{r1} may shift from their initial positions to ensure the local charge balance. Therefore, this local modification of the "octahedral sheet" induces lattice distortions which can affect the material to a great extent. These distortions can explain the diffuse scattering in the shape of a butterfly, joining the fundamental diffraction spots (0 2) to (1, 3) and (1 1) to (1 3)..., which are visible for the sample transformed at 28%, in Fig. 3b. This distortion can also explain the rapid change of the silicon environment seen by MAS NMR [3] on this same sample from Q_3 (silicon cation has three other cations in its nearest environment) towards Q_4 (silicon cation has four other cations).

For the removal of the second molecule of water, the dehydrolysis reaction can be written as:

$$2(OH)\{\text{with } 2Al^{V} \text{ in the nearest environment}\} \rightarrow H_2O(\uparrow) + O_{r2}\{\text{with } 2Al^{IV}\} \quad (2)$$

The four coordinated aluminium formed are also detected in NMR spectra [3, 14]. The "octahedral sheet" is reorganized, inducing the apparition of an isotropic halo in the diffraction diagram (Fig. 3d). This halo can be explained by a disordered aluminium distribution (Al–Al mean distance is about the same as the distance 0.4 nm measured from the halo), and NMR detected four-coordinated aluminium but also five- (30%) and six- (10%) coordinated aluminium in the same sample [3]. The new structural configuration of the O–Al bonds would permit a rotation of SiO_4 tetrahedra. This could explain the decrease of a and b parameters. The high local distortion of the SiO_4 sheet could explain the shift and the broadening of the Q_4 signal of silicon in NMR [3]. Thus the structure retains a long-range two-dimensional periodicity, which is seen on lattice imaging (Fig. 4), with a local high distortion.

The new interlayer period at about 1.2–1.3 nm observed on lattice imaging can be interpreted as being due to the new bonds between aluminium atoms and oxygen of the next tetrahedral sheet which form the population of six- and five-coordinated aluminium as detected by NMR [3, 14]. In such a way, the metakaolinite "layers" have a thickness of approximately two kaolinite layers (six layers of oxygen atoms). The steric condition of environment implies a partial penetration of the remaining oxygen atoms of the octahedral sheet in the cavity of the adjacent tetrahedral sheet. This condition may link two adjacent kaolinite layers. The lateral extension of this kind of "polymerization" between each of the two former layers is only about 5 nm (Fig. 8).

More precise information about this "*structure*" would require a systematic study by X-ray scattering on metakaolinite obtained from a pure, well-crystallized kaolinite sample.

4.2. Dehydroxylation mechanism

Only two phases are observed during the dehydroxylation: the obtained metakaolinite and the untransformed kaolinite. We did not observe, as by NMR [3], any intermediate state between the beginning and the end of dehydroxylation (removal of 1 or $2H_2O$ by aluminium).

The lattice imaging (Figs 5 and 6) has shown that the more favourable sites for starting dehydroxylation are the stacking defects and dislocations within the layers. In such domains with defects, the dehydroxylation reaction is easy and homogeneous. However, in the well-crystallized domains, the only favourable sites are the edges of the layers. Thus one can observe a reaction front (dashed line in Fig. 7) which progresses slowly. Such results explain why the shape of CRTA curve, as previously discussed [1], is significant in the two kinetic processes as a function of temperature, although this method is known to induce a very homogeneous reaction in the whole sample.

5. Conclusion

TEM observations of the heated samples at different transformation steps by CRTA allow each sample to be shown on different scales. Thus, it is possible to relate structures to local results obtained from NMR

and also to macroscopic processes as identified from the shape of the CRTA curves.

We observe only, and simultaneously, two phases (the original kaolinite and the metakaolinite), although CRTA would permit the identification of any intermediate state if it exists. Metakaolinite appears and progresses at defects of the original phase. Metakaolinite is not an amorphous material: it has a quasi-hexagonal periodic structure in the (*a*, *b*) plane. Along the *c** axis, metakaolinite consists of planar entities which result from the combination of two successive dehydroxylated sheets with a spacing of 1.2–1.3 nm.

Acknowledgements

This work was supported by the Fonds Régional de la Maitrise de l'Energie-Région Centre, France, and is based, in part, on the thesis submitted by Pascal Dion for the PhD in Chemical Physics, University of Orleans, France (1994).

References

1. P. DION, Thesis, University of Orléans (1994).
2. P. DION, D. ORTEGA, F. ROUQUEROL, J. F. ALCOVER and F. BERGAYA, submitted to *Clay Minerals*.
3. D. MASSIOT, P. DION, J. F. ALCOVER and F. BERGAYA, *J. Am. Ceram. Soc.* (1995) *J. Amer. Cer. Soc.* **78** (1995) 2940.
4. S. W. BAILEY, "Crystal structures of Clay minerals and their X Ray identification", Edited by G. W. Brindley and G. Brown (Mineralogical Society, London, 1980) p. 31.
5 D. L. BISH and R. B. VON DREELE, *Clays Clay Mineral* **37** (1989) 289.
6. J. ROUQUEROL, *Thermochim. Acta* **144** (1989) 209.
7. M. RAUTUREAU and M. STEINBERG, *J. Micros. Electron.* **10** (1985) 181.
8. C. TCHOUBAR, M. RAUTUREAU, C. CLINARD and J.-P. RAGOT, *J. Microsc.* **18** (1973) 147.
9 A. PLANCON and C. TCHOUBAR, *Clays Clay Mineral* **25** (1977) 436.
10. G. W. BRINDLEY, J. H. SHARP, J. H. PATTERSON and N. B. N. ACHAR, *Am. Mineral.* **52** (1967) 201.
11. B. SONUPARLAK, A. M. SARIKAYA and I. A. AKSAY, *J. Am. Ceram. Soc.* **70** (1987) 837.
12. K. SRIKRISHNA, G. THOMAS, R. MARTINEZ, M. P. CORRAL, S. DE AZA and J. S. MOYA, *J. Mater. Sci.* **25** (1990) 607.
13. V. A. DRITS, G. BESSON and F. MULLER, *Clays and Clay Min.* **43** (1995) 718.
14. J. F. LAMBERT, W. S. MILLMAN and J. J. FRIPIAT, *J. Am. Chem. Soc.* **111** (1989) 3157.

Received 23 October 1995
and accepted 24 April 1996